A Fault Diagnosis and Reconfiguration Strategy for Self-Validating Hydrogen Sensor Array Based on MWPCA and ELM

KAI SONG[1], (Senior Member, IEEE), PENG XU[1], YINSHENG CHEN[ID][2], (Member, IEEE), TINGHAO ZHANG[1], GUO WEI[1], AND QI WANG[1], (Member, IEEE)

[1]School of Electrical Engineering and Automation, Harbin Institute of Technology, Harbin 150080, China
[2]Department of Technique and Instrumentation of Measurements, Harbin University of Science and Technology, Harbin 150080, China

Corresponding author: Peng Xu (14B901016@hit.edu.cn)

ABSTRACT The flammable and explosive property of hydrogen is the main danger in its safe use, storage and transportation. In this paper, a novel hydrogen monitoring system is designed based on the principle of semiconductor, catalytic combustion and heat-conducting gas sensors. Also, the gas sensor will inevitably fail due to the nature of gas sensitive materials in the long-time monitoring process. To ensure the accuracy and reliability of hydrogen concentration measurement, a novel fault diagnosis and reconfiguration strategy for hydrogen sensor array based on moving window principle component analysis and extreme learning machine (MWPCA-ELM) is proposed. Firstly, online multiple faults detection is carried out by using MWPCA. Once one or multiple faults are detected, the measured values of other fault-free sensors will be used to recover the faulty data in real-time by using ELM predictor according to the relevancy among the hydrogen sensors. Secondly, the hydrogen concentration is reconfigured seamlessly and accurately based on ELM under the condition of small calibration data sample. Finally, fault diagnosis is conducted by MWPCA feature extraction coupled with ELM multi-classifier. In order to illustrate the effectiveness and feasibility of the proposed fault diagnosis and reconfiguration strategy, a hydrogen concentration monitoring experimental system was established. The average relative error (ARE) of hydrogen concentration estimation is declined from 1.18% to 0.82% compared with the traditional regression methods. Particularly, the proposed fault reconfiguration model can recover the fault data even if the concentration is changed, and the accuracy of fault diagnosis is 100% within 250 samples.

INDEX TERMS Fault diagnosis, reconfiguration, hydrogen sensor, extreme learning machine, moving windows principle component analysis.

I. INTRODUCTION

With the gradual depletion of petrochemical resources and the development of hydrogen industry, the hydrogen detection plays a prominent role throughout the fields of energy, metallurgy, national defense and chemical industry. As a kind of clean energy, hydrogen will only generate water after burning. Unfortunately, hydrogen is a flammable and explosive gas, whose flammable limits are nearly $4 \sim 94\%$ vol. The rapid and quantitative hydrogen concentration

The associate editor coordinating the review of this article and approving it for publication was Francesco Tedesco.

detection is imminent in the aerospace, navy and national defense fields [1]. For example, the process of water electrolysis hydrogen produces large amounts of hydrogen and oxygen. Hydrogen provides clean energy for the aerospace equipment or underwater equipment and oxygen affords the life security. There are also many dangerous situations caused by hydrogen leakage in the aircraft and submarines [2], [3]. In order to ensure the safety of the working environment and prevent explosion risks, it is essential to monitor the concentration of hydrogen quantitatively.

According to the different working principles, hydrogen sensors mainly include semiconductor type, catalytic

IEEE *Access*

K. Song *et al.*: Fault Diagnosis and Reconfiguration Strategy for Self-Validating Hydrogen Sensor Array Based on MWPCA and ELM

combustion type and thermal conductivity type. The semiconductor hydrogen sensor is mainly based on SnO_2, Fe_2O_3 and other materials. The hydrogen measuring the change of the sensor's gas-sensitive resistor. It is a low-cost hydrogen sensor with the advantages of quick response and high sensitivity [4]–[6]. The main disadvantage of semiconductor components is that the sensor's response to hydrogen is non-linear, and it is easy to be affected by environmental temperature and humidity. It is almost saturated in the case of high hydrogen concentration, so it can only be hydrogen concentration, so it can only be used in the case of very low concentration. Catalytic combustion catalyzed by precious metals such as platinum and palladium. According to the principle of catalytic combustion effect, the two arms of the bridge are composed of the detection element and the compensation element. When hydrogen is detected, the resistance of the detection element increases, and the output voltage of the bridge path changes. The output of the sensor is nearly linear with the concentration of hydrogen. The sensor is insensitive to the temperature and humidity of the environment due to the use of compensation elements. Its disadvantage is that the element is susceptible to sulfide, halogen compounds and other effects of poisoning, reduce the service life, in the high concentration of oxygen measurement error is large. The heat-conducting hydrogen sensor is made of platinum wire, which is based on the principle of gas thermal conductivity change. When the hydrogen concentration changes, the output voltage of the bridge also changes, and the voltage variable increases proportionally with the increase of the hydrogen concentration. Thermal conductivity hydrogen sensor integrated temperature compensation, with small drift, low power consumption, easy integration and other characteristics, and a wide range of concentration measurement, commonly used to detect high concentration of hydrogen content. However, the output signal is weak and the sensitivity is low, and the thermal conductivity does not change significantly at a low concentration. Therefore, combining the three types of hydrogen sensor concentration measurement ranges can provide a new solution for the seamless and accurate measurement of hydrogen concentration.

However, due to the characteristics of hydrogen sensor's gas-sensitive material, it is easy to be affected by external interference and its own fault in the long-term monitoring process, leading to a decrease in the accuracy and reliability of the measurement [7]. In the process of concentration monitoring, it is urgent to realize the working state and performance monitoring of hydrogen sensor. The self-validating sensor technology is a good choice to implement this requirement [8]. The concept and model of self-validating sensor are proposed by Clark and Henry, Oxford University in 1993 [9], [10]. Self-validating sensor can not only output the measured values, but also perform fault detection and isolation, fault diagnosis, fault recovery and working state evaluation, etc. In 2001, British Standards Institution established self-validating sensor technology as a standard, which defined the parameters for measuring data quality and

working state detailly. There is abundant information which is used to describe the work state in this kind of sensors. Thus, the reliability and maintainability of the sensor system is improved.

In the past, the contributions to the theories and applications of self-validating sensor have been made substantially by researchers from all over the world. Shen et al. proposed a multifunction self-validating sensor based on PCA and RVM [11]. However, the issue of multiple fault isolation is not considered. The historical information of the faulty sensor is used for fault recovery and the correlation among sensors is not taken into consideration. This method can only achieve short-term recovery. If the concentration changes, the recovery method will be invalid. Multiple fault recovery is not considered as well. Chen et al proposed EEMD for fault detection isolation and diagnosis [12], but the fault recovery is not considered. Yang et al. proposed a SNMF-SMVR for fault detection, isolation and recovery [13]. The idea of fault recovery is based on time series, which is the same as reference [11]. When the concentration changes, the problem of fault recovery is still unable to be eliminated. To summarize, the traditional fault detection, recovery and diagnosis face the dilemma in multiple fault isolation and recovery.

Extreme learning machine (ELM) [14]–[16] is a machine learning algorithm for single layer feedforward neural network (SLFN). The mainly feature is the parameters of hidden layer nodes can be random or given artificially and there is no need to adjust the parameters. The learning process only needs to calculate the output weight. ELM is widely used in classification, regression, clustering, and feature learning for its high learning efficiency and generalization ability [17]–[20].

Moving window principle component analysis (MWPCA) is a kind of feature extraction and fault detection method which employs moving window to deal with the data [21]–[24]. Since the hydrogen sensor faced the problem of small signal detection, moving window is better at small variations. Thus, MWPCA can more easily find the principal components which contain abnormal information ignored by PCA and KPCA [25]–[28].

In order to ensure the accuracy and reliability of hydrogen concertation measurement, self-validating sensor technology is introduced into the field of hydrogen concentration monitoring. Because the working principles of different sensors are different, the selection and design of self-validating algorithm are quite different. Based on the basic principle of hydrogen concentration measurement by gas sensor array, a self-validating hydrogen sensor array is presented in this paper. Aiming at the hardware result and measuring principle of sensor array, this paper presents a fault diagnosis and reconfiguration strategy for hydrogen sensor array based on moving window principle component analysis and extreme learning machine (MWPCA-ELM). The accuracy and reliability of hydrogen sensor is of great significance to ensure the safety of industrial production. It is necessary to detect the working state and performance of the sensor and recover the

K. Song *et al.*: Fault Diagnosis and Reconfiguration Strategy for Self-Validating Hydrogen Sensor Array Based on MWPCA and ELM

IEEE *Access*

faulty data to obtain the best estimated value, especially under the inconvenient changed conditions. The hydrogen concentration is measured seamlessly and accurately based on ELM under the condition of small calibration data sample. Online multiple fault detection of hydrogen sensor is carried out by using MWPCA. Once one or multiple faults are detected, the other fault-free sensors will be utilized to recover the faulty data in real-time by using ELM predictor according to the relevancy among the sensitive elements in the sensor array. Even if the concentration changes, the recovery accuracy will not be affected. A fault diagnosis algorithm based on MWPCA feature extraction and ELM multi-classifier is employed to identify the hydrogen sensor faults for the subsequent maintenance decisions.

Based on some previous work on hydrogen detection [29], [30], sensor fault detection, diagnosis and recovery [31]–[33], the objective of this paper is to achieve quantitative measurement of hydrogen concentration at high accuracy, and especially at high reliability. In Section II, the fundamental principle of ELM and MWPCA is analyzed. In Section III, the selection of hydrogen sensor and calibration data is analysis, as well hydrogen detection model under small sample of calibration data is built by using ELM regression model to realize the seamless and quantitative hydrogen concentration monitoring. In Section IV, the self-validating method is analysis. Given that the sensor fault may occur in the hydrogen concentration measurement process, MWPCA with squared prediction error (SPE) statistic is used to detect the fault in real time. To remove the influence of sensor fault for concentration measurement, ELM predictor is used to achieve the fault recovery. This method can online recover the output of fault sensor by using the relevance of the fault-free sensors. To identify the sensor fault type after fault detection and recovery, a fault diagnosis method based on MWPCA feature extraction and ELM multi-classifier is employed. In Section V, comparative analysis and experimental results for the proposed methodology and the conventional methods are investigated. Finally, the conclusion is accounted in Section VI.

II. FUNDAMENTAL THEORY

A. EXTREME LEARNING MACHINE

Extreme learning machine (ELM) is a generalized SLFN. Compared with SLFN, the training time of ELM is shorter and it is not easy to fall into the local minimum point [14]–[16]. The weights and biases are random initialized in ELM. There is no need to adjust the input weights and biases during the training process. As a result, the unique optional result can be achieved by setting the number of hidden layer neurons. Compared with the traditional methods, ELM has the advantages of fast learning and good generalization performance. [14]–[16]

The structure of traditional SLFN is shown as Figure 1. It is composed of input layer, hidden layer and output layer. The network is a completely connected network. The input
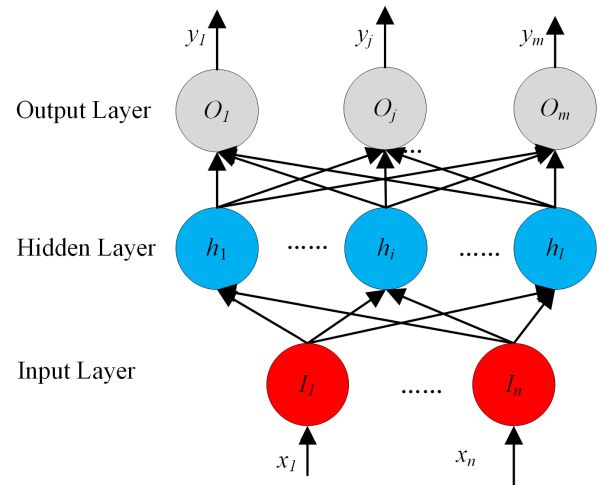
FIGURE 1. Structure of single layer feedforward neural network.

layer contains n neurons, corresponding to *n* input variables. There are *i* neurons in the hidden layer. The output layer has *m* neurons, corresponding to *m* output variables. The weights *W* between input layer and hidden layer are set as

$$W = \begin{bmatrix} w_{11} & w_{12} & \cdots & w_{1n} \\ w_{21} & w_{22} & \cdots & w_{2n} \\ \vdots & \vdots & \ddots & \vdots \\ w_{l1} & w_{l2} & \cdots & w_{ln} \end{bmatrix} \quad (1)$$

where w_{ji} represents the weight between *i*th neuron in input layer and the *j*th neuron in hidden layer.

The weight β between hidden layer and output layer is shown as

$$\beta = \begin{bmatrix} \beta_{11} & \beta_{12} & \cdots & \beta_{1m} \\ \beta_{21} & \beta_{22} & \cdots & \beta_{2m} \\ \vdots & \vdots & \ddots & \vdots \\ \beta_{l1} & \beta_{l2} & \cdots & \beta_{lm} \end{bmatrix} \quad (2)$$

where β_{ji} represents the weight between the *j*th neuron in hidden layer and *k*th neuron in output layer.

The bias *b* of neuron in hidden layer is set as

$$b = \begin{bmatrix} b_1 \\ b_2 \\ \vdots \\ b_l \end{bmatrix}_{l \times 1} \quad (3)$$

Set the input matrix *X* and the output *Y* of *Q* samples as

$$X = \begin{bmatrix} x_{11} & x_{12} & \cdots & x_{1Q} \\ x_{21} & x_{22} & \cdots & x_{2Q} \\ \vdots & \vdots & \ddots & \vdots \\ x_{n1} & x_{n2} & \cdots & x_{nQ} \end{bmatrix}_{n \times Q}$$

$$Y = \begin{bmatrix} y_{11} & y_{12} & \cdots & y_{1Q} \\ y_{21} & y_{22} & \cdots & y_{2Q} \\ \vdots & \vdots & \ddots & \vdots \\ y_{m1} & y_{m2} & \cdots & y_{mQ} \end{bmatrix}_{m \times Q} \quad (4)$$

IEEE *Access*

K. Song *et al.*: Fault Diagnosis and Reconfiguration Strategy for Self-Validating Hydrogen Sensor Array Based on MWPCA and ELM

Activation function in hidden layer is set as $g(x)$. The output of the network is known as

$$T = \begin{bmatrix} t_1 & t_2 & \cdots & t_m \end{bmatrix}_{Q \times m}, \quad (j = 1, 2, \cdots, m) \quad (5)$$

$$t_j = \begin{bmatrix} t_{1j} \\ t_{2j} \\ \vdots \\ t_{mj} \end{bmatrix}_{m \times l} = \begin{bmatrix} \sum_{i=1}^{l} \beta_{i1} g(w_i x_j + b_i) \\ \sum_{i=1}^{l} \beta_{i2} g(w_i x_j + b_i) \\ \vdots \\ \sum_{i=1}^{l} \beta_{im} g(w_i x_j + b_i) \end{bmatrix}_{m \times l},$$

$$(j = 1, 2, \cdots, m) \quad (6)$$

where $w_i = [w_{i1}, w_{i2}, \cdots, w_{in}]$ and $x_j = [x_{1j}, x_{2j}, \cdots, x_{nj}]$.

Thus Eq. (5) can be renew as

$$H\beta = T' \quad (7)$$

where T' is the transposition of T and H is the output matrix of hidden layer in the neuron network.

$$H(w_1, w_2, \cdots, w_l, b_1, b_2, \cdots, b_l, x_1, x_2, \cdots, x_l)$$
$$= \begin{bmatrix} g(w_1 \cdot x_1 + b_1) & g(w_2 \cdot x_1 + b_2) & \cdots & g(w_l \cdot x_1 + b_l) \\ g(w_1 \cdot x_2 + b_1) & g(w_2 \cdot x_2 + b_2) & \cdots & g(w_l \cdot x_2 + b_l) \\ \cdots & \cdots & \ddots & \cdots \\ g(w_1 \cdot x_m + b_1) & g(w_2 \cdot x_m + b_2) & \cdots & g(w_l \cdot x_m + b_l) \end{bmatrix}_{m \times l} \quad (8)$$

Given Q different samples $\{x_i, t_i\}$ and a standard SLFN with l hidden nodes and activation function $g(x)$ which is infinitely differentiable in any interval. For random chosen $w_i \in R^n$ and $b_i \in R$, the hidden layer output matrix H of the SLFN is invertible and $\|H\beta - T'\| = 0$.

Given any small positive value $\varepsilon > 0$ and activation function $g(x)$ which is infinitely differentiable in any interval, there exists $\hat{N} \leq N$, such that for N different samples $\{x_i, t_i\}$ and any $w_i \in R^n$ and $b_i \in R$ randomly chosen from any intervals, according to any continuous probability distribution, then with probability one, $\|H_{N \times \tilde{N}} \beta_{\tilde{N} \times m} - T_{N \times m}\| < \varepsilon$.

If the number of hidden layer neuron is equal to that of training samples, for any w and b, SLFN can approximate the training samples with zero error.

$$\sum_{j=1}^{Q} \|t_i - y_i\| = 0 \quad (9)$$

where $y_j = \begin{bmatrix} y_{1j} & y_{2j} & \cdots & y_{mj} \end{bmatrix}^T (j = 1, 2, \cdots, Q)$.

However, when the number Q of training sample is large, in order to reduce the amount of computation, the number of neurons in hidden layer is usually smaller than Q. The training error approximates to $\varepsilon > 0$.

$$\sum_{j=1}^{Q} \|t_i - y_i\| < \varepsilon \quad (10)$$

Therefore, when the activation function $g(x)$ is infinitely differentiable, there is no need to adjust all the parameters of SLFN. w and b can be random chosen before training and remain unchanged during the training process. The weight β between hidden layer and output layer can be obtained by solving the least squares solution of equation set.

$$\min_{\beta} \|H\beta - T'\| \quad (11)$$

The solution is described as

$$\hat{\beta} = H^+ T' \quad (12)$$

where H^+ is the Moore-Penrose generalized inverse of the hidden layer output matrix H.

For ELM classification, β can be transformed into the following optimization problem.

$$\min V_{ELM} = \frac{1}{2} \|\beta\|^2 + \frac{\lambda}{2} \sum_{i=1}^{N} \|\varepsilon_i\|^2$$
$$h(x_i)\beta = t_i - \varepsilon_i, \quad l = 1, 2, \cdots, N \quad (13)$$

where ε_i is the training error, λ is the penalty factor. According to Karush-Kuhn-Tucker theorem, Eq. (13) can be changed to

$$V_{ELM} = \frac{1}{2} \|\beta\|^2 + \frac{\lambda}{2} \sum_{i=1}^{N} \|\varepsilon_i\|^2 - \sum_{l=1}^{N} \sum_{j=1}^{m} a_{lj}(h(x_i)\beta_j - t_{ij} + \varepsilon_{ij}) \quad (14)$$

The optimum solution of Eq. (14) is

$$\beta = H^T \left(\frac{I}{\lambda} + HH^T \right)^{-1} T \quad (15)$$

The decision function is

$$label(x) = \arg \max_{i \in \{1, 2, \cdots, m\}} f_i(x) \quad (16)$$

B. MOVING WINDOW PRICIPLE COMPONENT ANALYSIS

PCA is a statistical method which applying multiple variable to obtain the key information. PCA utilizes variance analysis to deal with the obtained historical data. To improve the effectiveness of multivariate statistical, fault detection can be improved by data dimensionality reduction. If the measured data do not match with the principal component model, the fault can be detected in real time. [11]

MWPCA is a method which apply moving window to PCA to increase the detection ability. The adjacent several data are defined as a moving window. When new data is obtained, the last feature will be added into the moving window, as well the oldest feature is removed from the moving window. The window is updated in real time to improve efficiency and adaptability of the model. [21]

The moving window method is adding the current sampling result to the last $k - 1$ sampling data to form a new data sample x, whose window length is k. For ith time point,

K. Song *et al.*: Fault Diagnosis and Reconfiguration Strategy for Self-Validating Hydrogen Sensor Array Based on MWPCA and ELM
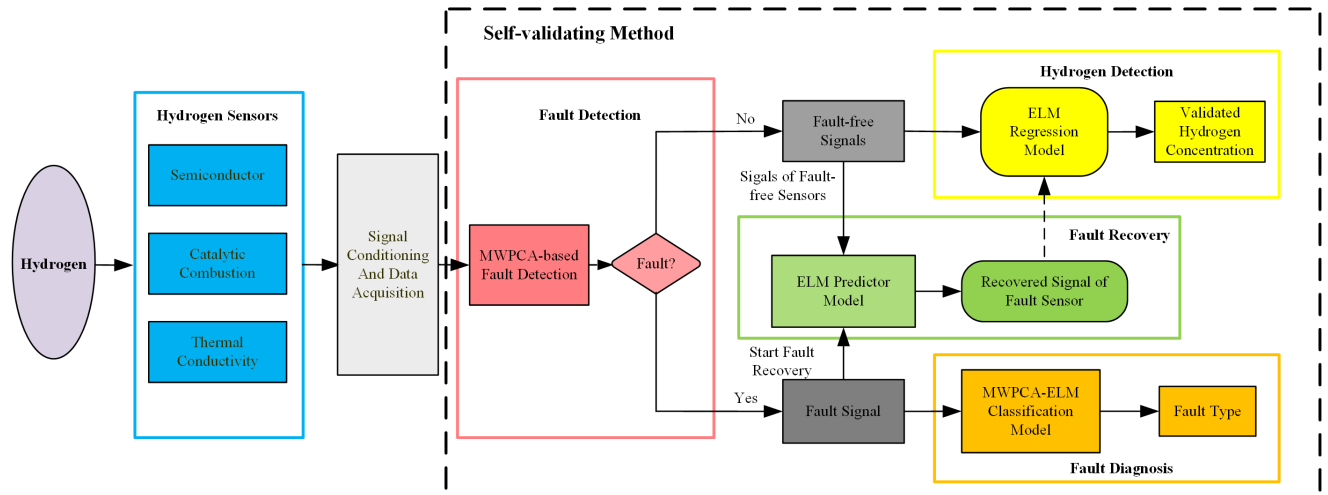
IEEE *Access*

FIGURE 2. Functional block diagram of proposed fault diagnosis and reconfiguration strategy for self-validating hydrogen sensor.

the sampling data x_i added to the moving window is shown as follow.

$$x_i' = x_i + x_{i-1} + \cdots + x_{i-k+1} \qquad (17)$$

Let ith sensor fail at the jth time point, the data of this point has been changed to $x_{ij} + \Delta b_{ij}$, where Δb_{ij} is the bias of fault. Let the length of moving window is k, the input is $x_{ij} + x_{i(j+1)} + \cdots + x_{i(j+k)} + \Delta b_{ij} + \Delta b_{i(j+1)} + \cdots + \Delta b_{i(j+k)}$. Since the input data has been normalized, the mean value is 0. The input is considered as $x_{ij} + \Delta b_{ij} + \Delta b_{i(j+1)} + \cdots + \Delta b_{i(j+k)}$. Compared with the original data, the bias has been increased.

III. PROPOSED FAULT DIAGNOSIS AND RECONFIGURATION STRATEGY

A. BASIC PROCEDURE OF PROPOSED STRATEGY

In order to obtain the reliable concentration results measured by the hydrogen sensor array composed of different types of hydrogen sensors, a self-validating algorithm for sensor array is designed. The functional block diagram of proposed fault diagnosis and reconfiguration strategy for self-validating hydrogen sensor array is shown in Figure 2.

Firstly, the MWPCA is modelled using the sensor array's redundant sensor measurements, and the fault is detected using SPE statistics. Secondly, the established MWPCA model is used for fault detection of hydrogen sensor array. Thirdly, the ELM regression model was modelled using sensor array measurements at different hydrogen concentrations. Once one or multiple faults are detected, the other fault-free sensors will be utilized to recover the faulty data in real-time by using ELM predictor according to the relevancy among the sensitive elements in the sensor array. Even if the concentration changes, the recovery accuracy will not be affected. A fault diagnosis algorithm based on MWPCA feature extraction and ELM multi-classifier is employed to identify the hydrogen sensor faults for the subsequent maintenance decisions.
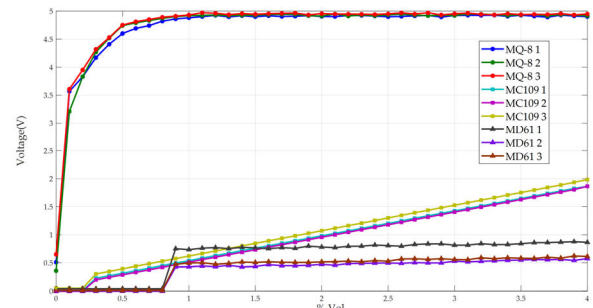

FIGURE 3. Sensitive properties of the nine hydrogen sensors.

B. HYDROGEN CONCENTRATION MEASUREMENT

1) SELECTION OF HYDROGEN SENSOR

In order to improve the detect accuracy, multiple sensors are used to measure hydrogen concentration. To achieve the quantitative hydrogen detection, three different types of hydrogen sensor produced by Hanwei Ltd. Co. are employed in this paper. To be specific, MQ8 series of semiconductor hydrogen sensor, MC109 series of catalytic combustion hydrogen sensor and MD61 series of thermal conductivity hydrogen sensor are adopted to measure hydrogen concentration for their different characteristics. In this paper, the above 3 types of hydrogen sensors are integrated into an array to measure the hydrogen concentration seamlessly.

In order to improve reliability of the system, the whole array contains 9 sensors. The number of each type sensor is three as shown in Table 1. Particularly, the 3 sensors' sensitivities are slightly different for accomplishing pattern recognition algorithm [29], [30], [34]. Figure 3 shows the sensitive properties of the 9 hydrogen sensors at different hydrogen concentrations. It can be seen that the output of each hydrogen sensor presents certain regularity in a certain concentration range. For example, the output of the semiconductor sensor approaches to saturation when the hydrogen concentration is greater than 0.8% vol. The output of the

IEEE *Access*

K. Song *et al.*: Fault Diagnosis and Reconfiguration Strategy for Self-Validating Hydrogen Sensor Array Based on MWPCA and ELM

TABLE 1. Selection of hydrogen sensor.

Type	Semiconductor			Catalytic Combustion			Thermal Conductivity		
Name	MQ8-1	MQ8-2	MQ8-3	MC109-1	MC109-2	MC109-3	MD61-1	MD61-2	MD61-3
Number	s_1	s_2	s_3	s_4	s_5	s_6	s_7	s_8	s_9

TABLE 2. Calibration samples of hydrogen concentration.

Hydrogen Sensor	Calibration Concentrations (% vol.)										
	0.1	0.2	0.3	0.4	0.5	0.6	0.8	1.0	2.0	3.0	4.0
Semiconductor	√	√	√	√	√	√	√	√	√	√	
Catalytic Combustion			√	√	√	√	√	√	√	√	√
Thermal Conductivity								√	√	√	√
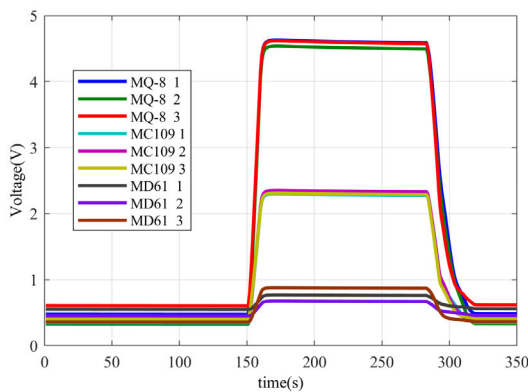
FIGURE 4. Response process of the nine hydrogen sensors.

FIGURE 5. The selection of calibrated samples number.

thermal conductivity is weak at the low concentration but it appears linear at the high concentration.

Figure 4 illustrates the response process of the 9 sensors. The test time is 350 s, and the sensor array is exposed to the test gas (hydrogen concentration is 2.5% vol) at 150 s. The work status is 26.3°C and RH 51.8%.

2) SELECTION OF CALIBRATION DATA
Here, calibration samples are determined by the gas-sensitive property and the concentration measuring range of each sensor. Experimental data of the sensor array response towards hydrogen concentration were obtained through the established calibration experimental system. In general, the more the number of calibration samples, the more accurate the gas concentration measurement. However, a large number of samples will greatly increase the difficulty and complexity of the calibration experiment.

Different pivotal concentration points were used to verify the influence between the calibrated sample size and the average relative error in the sensor array. The average relative errors to different sample points are described in Figure 5. The accuracy of detection is increasing while the calibrated samples size raises. When the sample size is 11, the detection accuracy is acceptable, so 11 samples are selected as training samples, which is shown in Table 2.
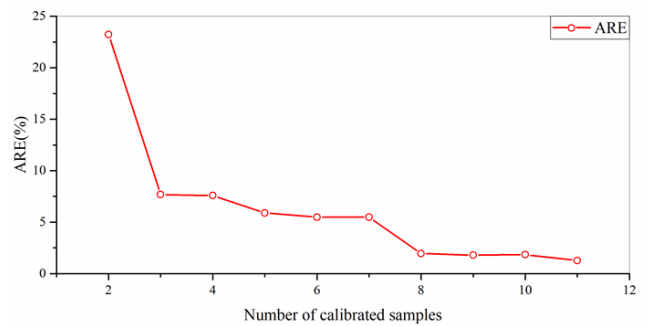
3) HYDROGEN CONCENTRATION MEASUREMENT USING ELM REGRESSION
This paper builds a novel regression model by using the small sample of hydrogen calibration concentrations and the 9-value outputs of the hydrogen sensor array. In this model, the hydrogen concentration is a nonlinear function of the 9 sensor outputs in the high-dimensional space. To reconstruct the hydrogen concentration, ELM regression is employed to fit the nonlinear mapping. Hence, the hydrogen concentration measurement is equivalent to the 9-value signal processing of the hydrogen sensor array. The detailed steps are shown as Table 3 and the input and output matrix is shown as Eq. (18).

$$P|T = \begin{bmatrix} MQ8 \begin{cases} V_{11} & \cdots & V_{1(11n)} \\ \vdots & \ddots & \vdots \\ V_{31} & \cdots & V_{3(11n)} \end{cases} \\ MC109 \begin{cases} V_{41} & \cdots & V_{4(11n)} \\ \vdots & \ddots & \vdots \\ V_{61} & \cdots & V_{6(11n)} \end{cases} \\ MD61 \begin{cases} V_{71} & \cdots & V_{7(11n)} \\ \vdots & \ddots & \vdots \\ V_{91} & \cdots & V_{9(11n)} \end{cases} \end{bmatrix} \begin{matrix} \\ C_1 \\ \vdots \\ C_{11n} \\ \\ \end{matrix} \quad (18)$$

where P is a $9 \times 11 \times n$ matrix, which represents the training input sample of the ELM regression model and

K. Song *et al.*: Fault Diagnosis and Reconfiguration Strategy for Self-Validating Hydrogen Sensor Array Based on MWPCA and ELM

IEEE *Access*

TABLE 3. Hydrogen concentration measurement using ELM regression.

Algorithm of hydrogen concentration measurement using ELM regression
Procedure:
1) Standardize the training samples and generate the training sample matrix *X*.
2) Random choose $w_i \in R^n$ and $b_i \in R$ before training.
3) Determine the number of hidden layer neuron and the activation function.
4) Calculate the weight β between hidden layer and output layer.
5) Calculate the hidden layer of output matrix *H*.
6) Calculate the output layer weight $\hat{\beta} = H^+ T'$.
7) Using the trained model to obtain the hydrogen concentration.

V_{ij} represent the output voltage of 3 kind of gas sensors in different concentrations. The range of *i* is 1,2,…,9, which means the 9 gas sensors. The value of *j* is $11 \times n$, which represents the concentration sampling point and *n* is the number of sampling point at the same concentration. *T* is the training output sample of the ELM regression model, which denotes the different concentrations.

C. FAULT DETECTION, RECOVERY AND DIAGNOSIS OF HYDROGEN SENSOR

The traditional hydrogen sensor can only output the measured hydrogen concentrations. After the sensor works for a long time, it is hard to judge whether the sensor's performance changes, whether the sensor output is correct and whether the sensor malfunctions. The ELM based online fault detection and recovery method proposed in this paper has the property of real-time fault detection. Not only can it correctly detect whether the sensor is faulty but also can recover the fault data in real time. To remain the normal running of the sensor system, the recovered sensor output is used to substitute the actual faulty signal over a period of time while the fault sensor is unable to be replaced in time. Hence, the reliability of the sensor system is improved.

1) FAULT MODE ANALYSIS OF HYDROGEN SESNOR

In the paper, 5 main faults are analyzed based on the long-term observation and the structure characteristic of the 3 kinds of hydrogen sensors. The detailed fault mode analysis is as follows:

(a) Impact Fault. Since the internal resistance of the hydrogen-sensitive sensor is high, the sensor output is susceptible to be disturbed by the external disturbance. Particularly, such interference is often of a short duration, and the sensor output shows a spike that lasts for only a short time as the impact fault.

(b) Broken-Circuit Fault. The broken-circuit fault is often caused by the broken signal electrode, the damaged measuring circuit, and the crack soldering. The sensor output will decrease rapidly to zero whereas it should have made some responses with the changes of hydrogen concentrations.

(c) Overloading Fault. The power voltage of the sensor system may have a bias which could result in the

overloading fault. Sometimes, the pollutants or interfering odors may also affect the sensor output. The output will become a large constant whereas it should have undertaken some changes with the changes of hydrogen concentrations.

(d) Invalidation Fault. In actual application, the hydrogen sensor may remain running in the long-term poor film may also lead to the fault. The output will maintain nearby constant whereas it should have changed a lot with the changes of the hydrogen concentrations.

(e) Abnormal Variance Fault. The sensor system is always exposed to the poor measured environment which will strongly affect the performance of the measuring circuit. For example, the damaged internal amplifier or the faulty signal conditioning circuit may also cause the abnormal variance fault. The output will become an abnormal fluctuation whereas it should have been very steady all the time.

Above 5 faults are simulated by adding the impact voltage, power bias and by removing the power supply to the normal signals, respectively [12], [29]. The normal signals (i.e. the fault-free signal) are the real-world measured output of the hydrogen sensor. Without loss of generality, take semiconductor hydrogen sensor MQ8-1 (S_1) for an example, 5 kinds of simulated fault signals are shown in Table 4 at the hydrogen concentration of 2000 ppm.

2) REAL-TIME FAULT DETECTION USING MWPCA

The primary *n*-dimensional sensor data space is replaced by *k*-dimensional subspace $\widehat{S}$ and the $(n-k)$-dimensional residual components subspace $\tilde{S}$. The SPE statistic in subspace $\hat{S}$ is defined as:

$$SPE = \left\| \tilde{C}\bar{x} \right\|^2 \leq \delta_{SPE}^2 \qquad (19)$$

where δ_{SPE} is the SPE threshold, which is decided by the sampling distribution of SPE. If the value of SPE is larger than δ_{SPE}, there will be a fault in the sensor array. The contribution determines the position of the fault sensor. The SPE contribution rate of the *j*th sensor at the *i*th time point is written as:

$$SPE_{ij} = e_{ij}^2 = (X_{ij} - \hat{X}_{ij})^2 \qquad (20)$$

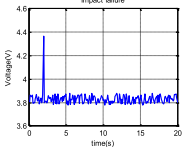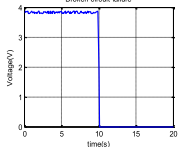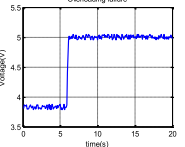The correlation coefficient matrix *R* is written as

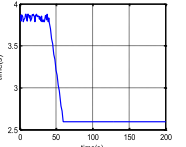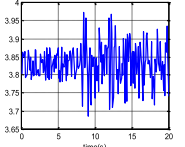$$R = UD_\lambda U^T \qquad (21)$$

where $D_\delta = \text{diag}(\lambda_i, i = 1, 2, \cdots, n)$ is the eigenvalue matrix and *U* is the eigenvector matrix.

Comparing with the contribution of each sensor, the reason that SPE is larger than the threshold will be found. In this way, the position of the fault sensor will be confirmed. The detailed algorithm of real-time fault detection is shown in Table 5.

3) ONLINE FAULT RECOVERY USING ELM PREDICTOR

To achieve the online fault recovery of hydrogen sensor, the ELM predictor is proposed in this paper. The outputs of fault-free sensors are used as inputs of the predictor to estimate the output of the fault sensor. As shown in Figure 6,

IEEE *Access*

K. Song *et al.*: Fault Diagnosis and Reconfiguration Strategy for Self-Validating Hydrogen Sensor Array Based on MWPCA and ELM

TABLE 4. Fault mode analysis.

| fault	Impact	Broken-circuit	Overloading	Invalidation	Abnormal variance
Feature	Output suddenly increases about 0.2 s	Output suddenly changes to 0	Output is the power voltage	Output is a constant	Output fluctuates distinctly
Reason	Output is disturbed by the external disturbance	Broken signal electrode or measuring circuit	Power voltage has a bias	Sensitive film is polluted	Exposed to poor environment
Wave form					
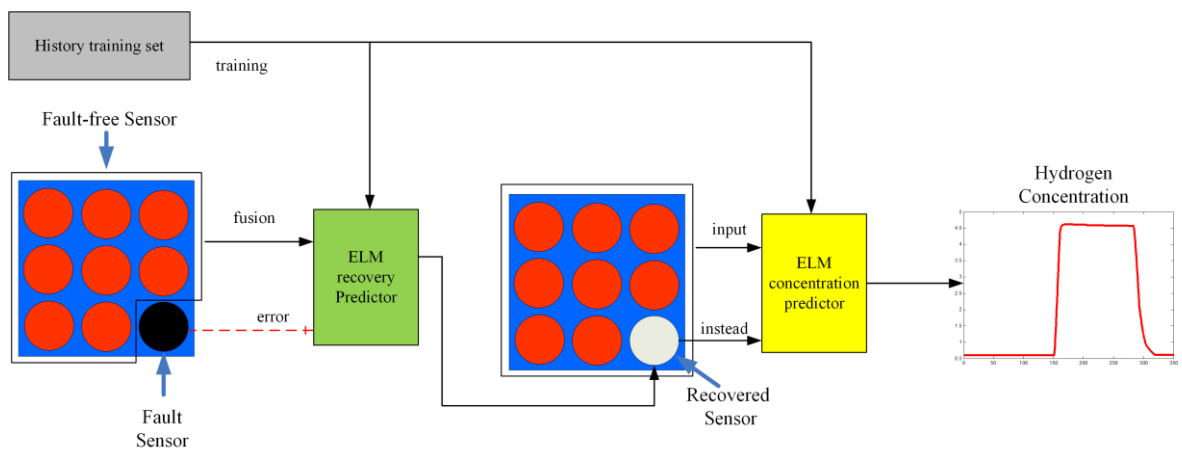
FIGURE 6. Fault sensor data recovery by using fault-free sensors and ELM.

TABLE 5. Real-time fault detection of hydrogen sensor using MWPCA.

Algorithm of hydrogen sensor real-time fault detection using MWPCA

Training process:
1) Choose fault-free history data and preprocess the data.
2) Calculate the mean and standard deviation of the data, and normalize the data to build the training sample.
3) Choose a window length k to obtain a new input matrix x'.
4) Calculate the eigenvalue and eigenvector of correlation coefficient matrix
5) Calculate the number of PCs.
6) Calculate the statistics SPE.
7) Calculate the threshold SPE_a.

Online fault detection process:
1) Acquire the sensor array response x_i in real time.
2) Normalize the data x_t to build the test sample.
3) Build the moving window input matrix x_{new}'.
4) Calculate the statistics SPE.
5) Judge whether the statistics SPE over the threshold Q_a or not. If the number is the larger than the threshold, the sensor is fault. If not, return to the step i to collect the next sample.

the incorrect output signal will be replaced by the estimated signal. Once the fault is eliminated, the ELM regression method which is built in section III. It will be employed again for the hydrogen concentration measurement by using the fault-free data and the recovered data.

Based on the long-term observation and gas-sensitive property analysis of the normal experimental data, the 9 hydrogen sensor outputs appear to be significant regulation with the changes of hydrogen concentrations, as is shown in Figure 3. Fault data can be recovered on the basis of the relevance of the above sensor data in the different concentration regions. According to the output voltage of all the sensors in the training samples, the relevance between any two sensors can be represented by Pearson correlation coefficient $r(x_j, x_k)$ as:

$$r(x_j, x_k) = \frac{Cov(x_j, x_k)}{\sqrt{Var(x_j) \cdot Var(x_k)}} \quad (22)$$

where x_j and x_k are the output signals of 9 hydrogen sensors, respectively. Table 6 shows the correlation coefficient of 9 different sensors while hydrogen concentration is 5000 ppm in the experiment. The relevance of 9 hydrogen sensors is apparent, which provides the possibility of fault data recovery.

If the multiple faults occur in the sensor array, the function of single-fault detection will be affected and even break down. Therefore, it is an important part to achieve the

K. Song *et al.*: Fault Diagnosis and Reconfiguration Strategy for Self-Validating Hydrogen Sensor Array Based on MWPCA and ELM

IEEE*Access*

TABLE 6. Correlation coefficient of 9 hydrogen sensors.

| Correlation coefficient		Semiconductor			Catalytic combustion			Thermal conductivity		
		MQ8-1	MQ8-2	MQ8-3	MC109-1	MC109-2	MC109-3	MD61-1	MD61-2	MD61-3
Semiconductor	1	1	0.9965	0.9990	0.5007	0.4941	0.5076	0.5608	0.5536	0.5567
	2	0.9965	1	0.9981	0.4865	0.4797	0.4941	0.5370	0.5298	0.5333
	3	0.9990	0.9981	1	0.4772	0.4705	0.4845	0.5213	0.5239	0.5274
Catalytic combustion	1	0.5007	0.4865	0.4772	1	0.9999	0.9998	0.7954	0.8407	0.8236
	2	0.4941	0.4797	0.4705	0.9999	1	0.9997	0.7922	0.8387	0.8207
	3	0.5076	0.4941	0.4845	0.9998	0.9997	1	0.7958	0.8410	0.8245
Thermal conductivity	1	0.5608	0.5370	0.5213	0.7954	0.7922	0.7958	1	0.9949	0.9973
	2	0.5536	0.5298	0.5239	0.8407	0.8387	0.8410	0.9949	1	0.9972
	3	0.5567	0.5333	0.5274	0.8236	0.8207	0.8245	0.9973	0.9972	1
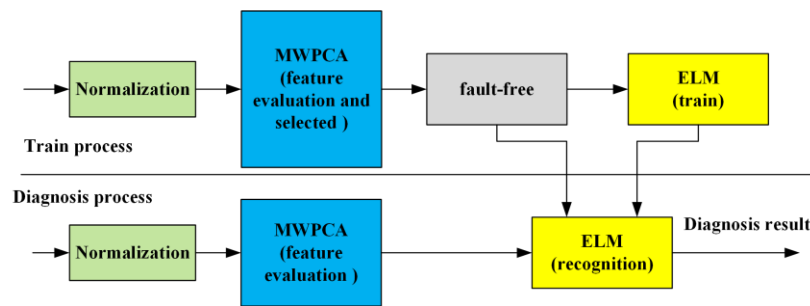
FIGURE 7. Sensor fault diagnosis based on MWPCA and ELM multi-classifier.

multi-fault recovery. The proposed method can utilize SPE to detect multiple-fault and use the data of fault-free sensors to recover the fault data.

$$P = \begin{bmatrix} V_{11} & V_{12} & \cdots & V_{1m} \\ V_{21} & V_{22} & \cdots & V_{2m} \\ \vdots & \vdots & \ddots & \vdots \\ V_{(9-n)1} & V_{(9-n)2} & \cdots & V_{(9-n)m} \end{bmatrix}^T \quad (23)$$

$$T = \begin{bmatrix} V_{11} & V_{12} & \cdots & V_{1m} \\ V_{21} & V_{22} & \cdots & V_{2m} \\ \vdots & \vdots & \ddots & \vdots \\ V_{n1} & V_{n2} & \cdots & V_{nm} \end{bmatrix}^T \quad (24)$$

where n is the number of faulty sensors in the array, m is the number of concentration samples, P is a $(9-n) \times m$ matrix which denotes the training input samples of the predictor, T is an $n \times m$ matrix which denotes the training output samples of the predictor, $V_{(9-n) \times m}$ and $V_{n \times m}$ represent the output voltage of different kinds of sensors in different concentrations, respectively. While the multiple sensors occur fault, the above ELM predictor is capable of recovering the fault data.

TABLE 7. Feature extraction using MWPCA.

Algorithm of MWPCA feature extraction
1) Standardize the training samples and generate the training sample matrix X.
2) Calculate the moving window input X'.
3) Calculate the feature vector and the eigenvalue of X'. Choose the feather vector whose eigenvalue's cumulative contribution rate is over 90%.
4) Calculate all PCs of the training samples on the selected feather vector and regard the projection as the feather vector of ELM multi-classifier. Put the test sample into the trained classifier to identify the sensor fault status.

4) FAULT DIAGNOSIS USING WMPCA FEATURE EXTRACTION AND ELM MULTI-CLASSIFIER

Fault diagnosis as an important function is the capable of determining the sensor fault type and providing the fault resolution. The abnormal state of the hydrogen sensor output signal presents the transient change that embodies some important fault information. In this paper, MWPCA is employed to realize the feature extraction of the faulty signal. The detailed steps of MWPCA feature extraction are given in Table 7 and the principle of fault diagnosis using ELM multi-classifier is shown in Figure 7.
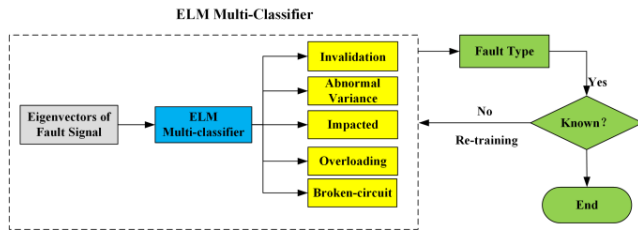
IEEE *Access*

K. Song *et al.*: Fault Diagnosis and Reconfiguration Strategy for Self-Validating Hydrogen Sensor Array Based on MWPCA and ELM

FIGURE 8. Structure design of ELM multi-classifier.

TABLE 8. ELM multi-classifier.

Algorithm of ELM Multi-Classifier
1) Standardize the fault samples to eliminate the impact of the dimension.
2) Code the five types of samples as 0,1,2,3,4,5, respectively as output of the five-classifier.
3) Random chosen the weight w and β.
4) Choose the activation function and the corresponding number of hidden neurons.
5) Apply the Theorem 2 to build the ELM training method.
6) Match the output of the predicted result and the expect result and calculate the accuracy.
7) If the accuracy is lower than 95%, repeat step 3 to step 6.

To identify the fault types of hydrogen sensors, this paper devised an ELM multi-classifier which was composed of a multi-classifier. As discussed above, the extracted feature vectors of faulty signals are used as input of the ELM multi-classifier. Given the 5 fault states such as invalidation, overloading, abnormal variance, impact and broken-circuit state, an ELM multi-classifier is built.

As shown in Figure 8, 5 kinds of fault types are recognized by ELM multi-classifier. If there are any new fault modes, the classifier needs to be trained again. Since the multi-classifier does not have the unrecognized domain, it has higher classification accuracy in practical application. Here, the multi-classifier is trained according to the training samples of the simulated 5 faults. The detailed process is shown in Table 8.

IV. EXPERIMENT AND RESULTS

To demonstrate the feasibility and effectiveness of the proposed strategy, an experimental system of hydrogen detection having hydrogen sensor fault detection, diagnosis and recovery functions was designed. The experiment of hydrogen detection was conducted under the hydrogen concentration ($0 \sim 4\%$ vol) and hydrogen sensor faults were simulated under the 5 common fault modes. To further verify the performance of the proposed strategy, the contrast experimental results of different methods using the same training and test samples were also given.

A. EXPERIMENTAL SETUP

The experimental system was mainly composed of hydrogen sensor array, gas source, gas chamber, intake device, power supply, data acquisition device and laptop PC as shown in Figure 9 and the physical picture of sensor system is shown in Figure 10. The hydrogen sensor array that consisted of 3 different types of hydrogen sensors, namely semiconductor,

catalytic combustion and thermal conductivity, was fixed in the gas chamber. The gas chamber temperature was maintained at 26.3°C.

The hydrogen was prepared according to the calibration samples in Table 2. Particularly, the different concentrations were confected by adjusting the mass flow controller (MFC). The electrical source supplied power for hydrogen sensor and circuits. Data acquisition device utilized a USB card (USB-2089, Art Co. Ltd.) with 16 analog inputs at up to 400 kHz and a 14-bit A/D conversion accuracy. The emulate faults were implemented by using MATLAB. Both this method and the contrast algorithm are tested by MI Air 13, whose CPU is Core i5-7200U, RAM is 8 GB. The software developed on the NI LabVIEW platform was used in gas-sensitive property analysis and calibration experiment of hydrogen sensor, and also provided a test platform for algorithm validation. The software system adopted the modular design which was composed of the following several modules, i.e. gas-sensitive property test, real-time monitoring of hydrogen concentration, fault detection, fault data recovery, fault diagnosis, measurement results display and saving. All the algorithms were independently prepackaged and integrated in the experimental system, which constituted a laptop-based hydrogen analyzer.

B. HYDROGEN CONCENTRATION MEASUREMENT

The first step of hydrogen detection is to build the training samples and the testing samples. In this experiment, the training samples contain 11 concentration points which are shown in Table 2. Each concentration point contains 10 samples. The testing samples contain 40 concentration points which range from 0.1% vol to 4% vol and the interval is 0.1% vol. As discussed in Section III, ELM regression model is used to measure the hydrogen concentration. The inputs of ELM regression model are 9-value outputs of the hydrogen sensor array, and the output is the hydrogen concentration. In this paper, the number of hidden layer neuron is selected as 20. Figure 11 shows the experimental results of hydrogen concentration measurement.

1) PERFORMANCE COMPARISON OF DIFFERENT METHODS

To further verify the concentration prediction performance of ELM, the comparison results using relevance vector machine (RVM) [11] and least square support vector machine (LSSVM) [29] and radial basis function neural networks (RBFNN) [35] for the same training and test samples are given in Table 9. Here, the parameter of the kernel function in RVM is 2.3. The parameter of the kernel function in LSSVM is 491 and the penalty factor is 24. The parameter of spread is 32. The number of input data is 9 and the number of output is 1.

Obviously, compared with RVM, LSSVM and RBFNN, this proposed method has highest average relative error (ARE) of concentration measurement. The reason is that the small training samples are insufficient for neural networks to perform a precise concentration estimator. From the view
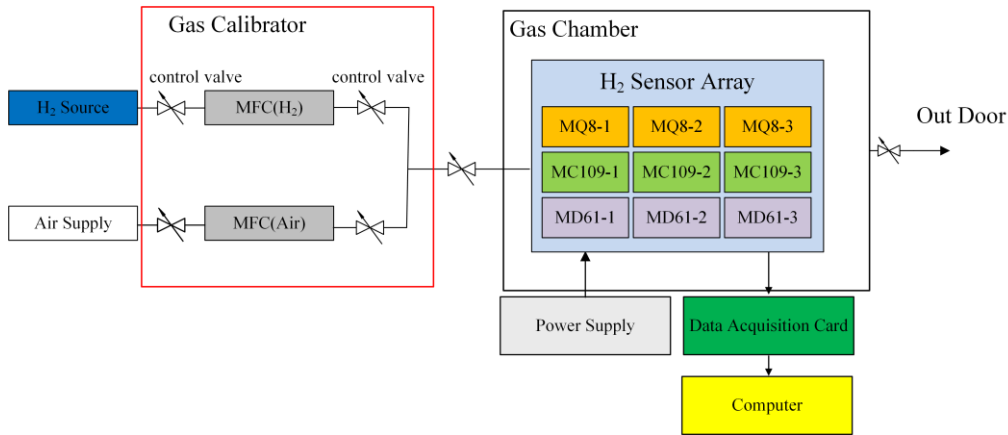
K. Song *et al.*: Fault Diagnosis and Reconfiguration Strategy for Self-Validating Hydrogen Sensor Array Based on MWPCA and ELM

IEEE *Access*

FIGURE 9. Experimental setup of hydrogen measurement system.
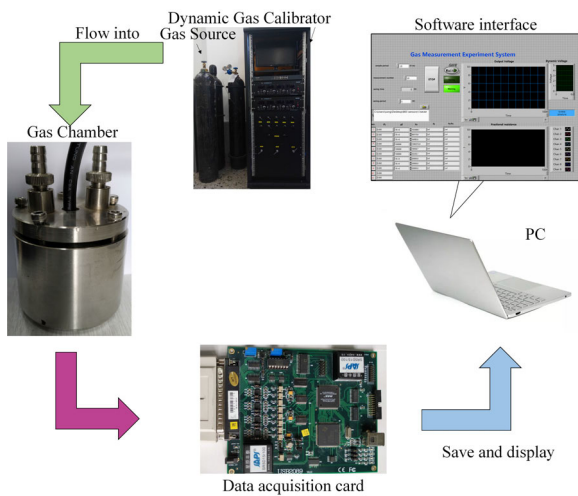
FIGURE 10. Experimental setup.

FIGURE 11. Hydrogen concentration measurement using the proposed ELM regression model and comparison results with several methods.

of statistical, ELM has better generalization ability in the case of small samples than RVM and LSSVM. Additionally, the training time of ELM is faster than the three compared methods because SLFN is applied in ELM.

TABLE 9. Performance comparison of different regression methods for hydrogen concentration measurement.

Method	Average relative error (%)	Training time(s)
RBFNN	2.16	0.70
LSSVM	1.18	0.15
RVM	1.31	0.29
ELM	0.82	0.02

2) IMPACT OF SENSOR NUMBER

Furthermore, the influence about the number of gas sensors in the sensor array is analyzed by employing 3, 6 and 9 gas sensors (the number of each type sensor is 1, 2, 3, respectively). The above 4 regression methods are used to measure the hydrogen concentration, and the measured results are shown in Figure 12. It is obvious that ARE is the lowest when 9 sensors are used while ARE is the largest when 3 sensors are employed. Thus, the gas sensors redundant method can further improve the accuracy of hydrogen concentration measurement.

C. REAL-TIME FAULT DETECTION
1) SINGLE FAULT DETECTION

The MWPCA method based on SPE statistic is studied to detect the 5 faults (i.e. invalidation, overloading, abnormal variance, impact and broken-circuit) of hydrogen sensors. In general, thermal conductivity hydrogen sensor MD61-1 (S_7) in the array is taken as an example. 5 typical faults are injected to simulate the fault experiment. The results of fault injection and MWPCA based SPE detection are shown in Figure 13. The blue line denotes the value of SPE. The red line is the corresponding threshold whose value is $SPE_\alpha = 7.07$.

Taken broken-circuit fault shown in Figure 13 (c) as an example, the sensor encounters broken-circuit fault at 10 s. The value of SPE increases sharply at this moment and exceeds the threshold, which proves that there will be a fault or more faults in the sensor array. The position of fault sensor
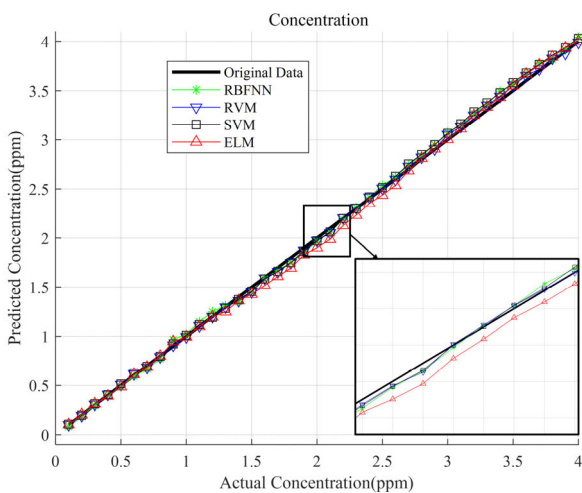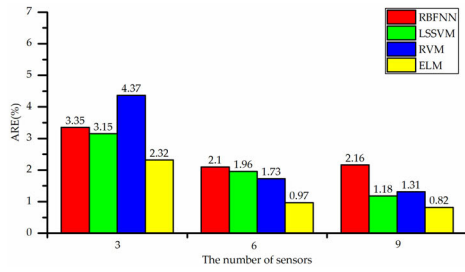
IEEE Access

K. Song *et al.*: Fault Diagnosis and Reconfiguration Strategy for Self-Validating Hydrogen Sensor Array Based on MWPCA and ELM

FIGURE 12. Average relative error of different methods under different numbers of hydrogen sensors.

can be determined according to their contributions for SPE value at the fault time. As shown in Figure 13 (c), the contribution of 7th sensor is the largest among all the sensors and it demonstrates that MD61-1 (S_7) is fault.

2) COMPARASON OF WMPCA AND PCA
Firstly, MWPCA accumulates the bias information in the moving window by utilizing moving window to ensure that more information is included in fault detection. Secondly, the contribution rate of the fault sensor is relatively larger and the accuracy of fault isolation is better. Therefore, the application of WMPCA will have better result. in fault detection than PCA.

Invalidating fault is taken as an example to verify the fault detection and isolation ability of WMPCA and PCA. As shown in Figure 14, the amplitude of the fault signal is small and the SPE statistics just exceed the threshold. The SPE contribution of S_7 at the fault time (6 s) (Figure 14(a))

of the fault sensor is larger than the other sensors by using WMPCA, which proved that S_7 is faulty. Therefore, the fault achieved. However, SPE contribution of S_7 at the fault time (Figure 14(b)) is not the largest yet, which means that the fault isolation is not achieved by using PCA. Therefore, although the effects of the fault detection based WMPCA and PCA are similar, the effect of the fault isolation based on WMPCA is better than PCA.

3) ANALYSIS OF CONCENTRATION CHANGE IMPACT
Figure 15 shows the response curve and the SPE statistic of the 9 hydrogen sensors when the hydrogen concentrations vary. It is obvious that the SPE value changes less and keeps lower than the threshold whereas the concentration changes greatly. Therefore, fault detection does not work when the hydrogen concentrations vary in the environment.

4) MULTIPLE SIMULTANEOUS FAULTS DETECTION
The conventional fault detection methods have difficulty in multi-fault isolation when multiple faults occur in the sensor array simultaneously [32]. The proposed WMPCA method is capable of detecting multiple faults in real time.

a: MULTIPLE FAULT OCCURRING AT DIFFERENT TIMES
According to Figure 16. The SPE of 2 s has a sudden change, which represent the actual impact fault of MD61-2 (S_8), whose SPE contribution rate is the highest. Starting from 6 s, the SPEs suddenly increase, and larger than the threshold SPE_α, which means some sensor is out of order.
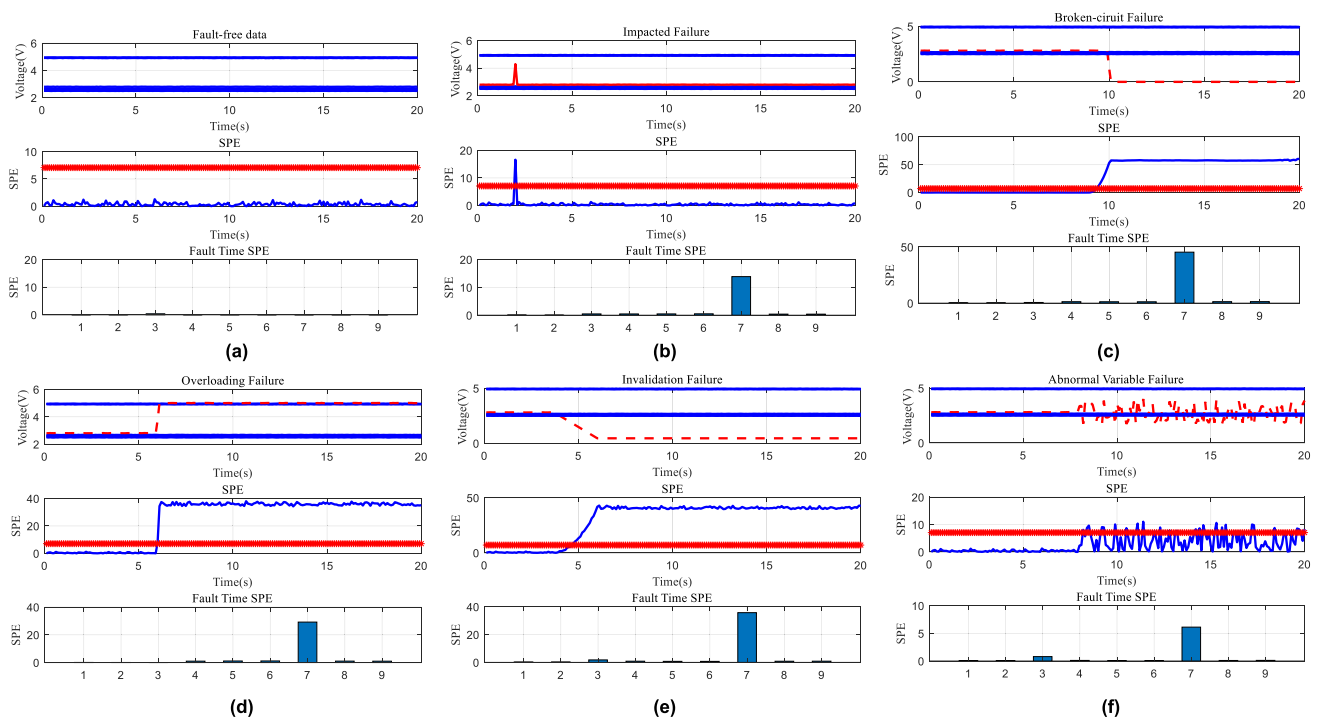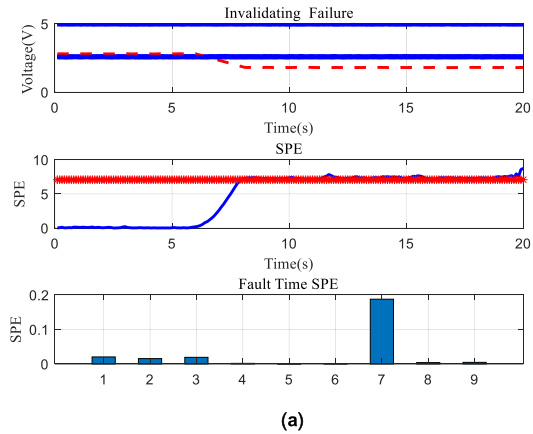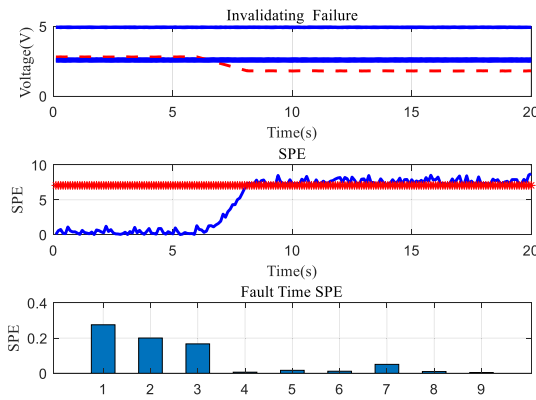

FIGURE 13. Hydrogen concentration Son measurement using the proposed ELM regression model and comparison results with several methods.

K. Song *et al.*: Fault Diagnosis and Reconfiguration Strategy for Self-Validating Hydrogen Sensor Array Based on MWPCA and ELM

IEEE *Access*

FIGURE 14. Comparison of WMPCA and PCA to fault detection (a) the result using WMPCA and (b) the result using PCA.

Another jump is started from 10 s, and the SPE is larger than SPEα too, which means another sensor is faulty at 10 s. The contribution rate is used to achieve fault isolation of the sensor array. The contribution rate of S$_7$ at 6 s is the largest, which proves S$_7$ is faulty. The contribution rates of S$_4$ and S$_7$ are the largest at 10 s, which proves that S$_4$ and S$_7$ are all fault at this moment. Therefore, multiple fault occurred at different times can be effectively detected.

b: MULTIPLE FAULT OCCURRING AT THE SAME TIMES

Without losing generality, the case that broken-circuit fault simultaneous occurring at 10 s at MD61-1 (S$_7$) and MD61-2 (S$_8$) is taken as an example and shown in Figure 17 (a). The case that overloading fault simultaneous happening at 6 s at MC109-1 (S$_4$) and MD61-1 (S$_7$) is taken as an example and shown in Figure 17(b). The sensor array will be faulty if the SPE statistic exceeds the threshold SPE$_\alpha$. According to the contributions of each sensor's SPE statistic at the fault time, the fault sensors can be determined and isolated. As can be seen in Figure 17(a), the contributions of S$_7$ and S$_8$ are larger than other sensors, it proves that these two sensors are faulty. S$_4$ and S$_8$ in Figure 17(b) are confirmed as the faulty sensors at the same way. Thus, this proposed method achieves real-time detection of multiple faults simultaneously.
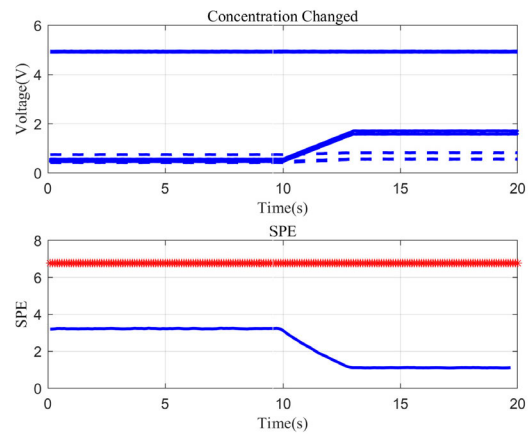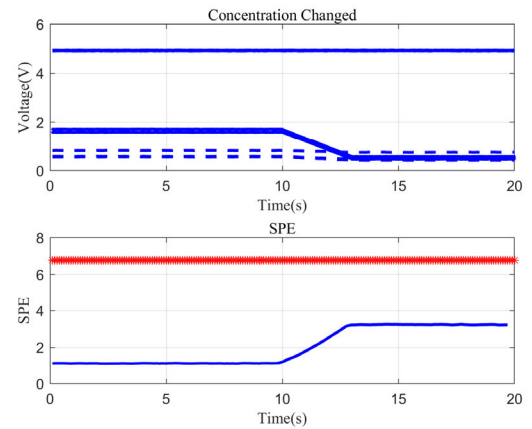
FIGURE 15. Response curve and SPE statistic of 9 hydrogen sensors when hydrogen concentrations change (a) from 1% vol to 3.5% vol and (b) from 3.5% vol to 1% vol.

D. ONLINE FAULT RECOVERY

1) SINGLE FAULT RECOVERY

As mentioned in Section III, the 8 fault-free sensors will be employed to recover the fault sensor output by using ELM predictor when the fault sensor is detected. Then, the faulty signal will be replaced by the predicted signal during the period of fault. To verify the performance of the proposed method, the fault recovery experiments under 5 fault types by utilizing ELM method is conducted. The predictor is updated online and the fault-free data are used to recovery the fault one. The kernel function of ELM predictor is sine, and the number of hidden layer node is 18. The training samples are the same as shown in Table 2. The faulty catalytic combustion hydrogen sensor MC109-1 (S$_4$) in the sensor array is taken as an example. The experimental results of real-time fault recovery are shown in Figure 18.

In order to check the performance of ELM recovery method, the RVM predictor mentioned in reference [36] is treated as the comparative experiment. It can be seen from Figure 16 that the performance of RVM and ELM are almost the same. The two methods are able to accomplish fault recovery for all the fault types and ARE is within 0.6%. The training time of ELM is 0.04 s and that of RVM is 0.16 s.
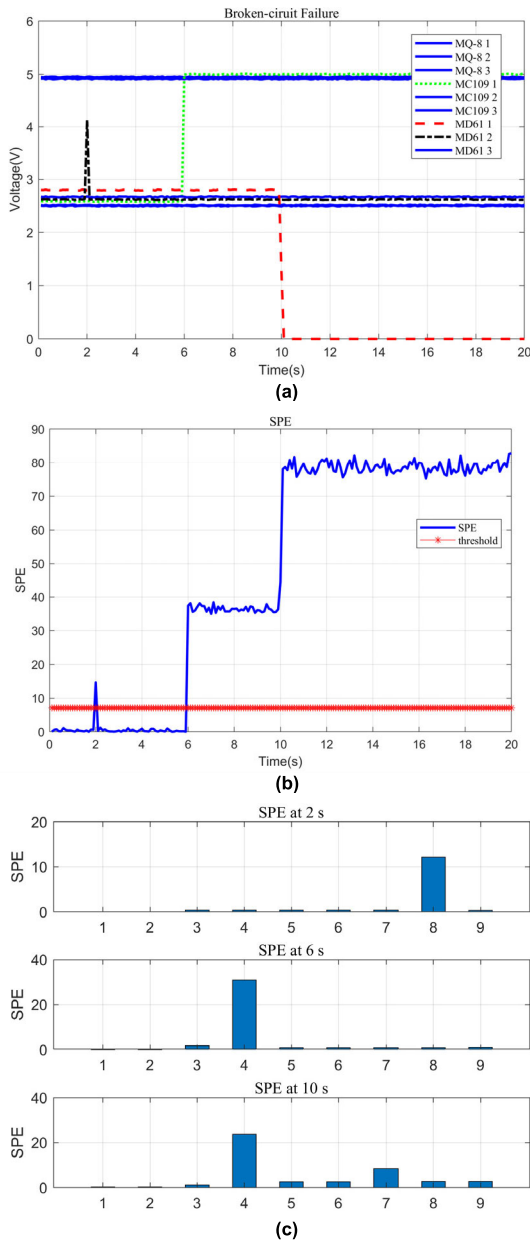
IEEE *Access*

K. Song *et al.*: Fault Diagnosis and Reconfiguration Strategy for Self-Validating Hydrogen Sensor Array Based on MWPCA and ELM

FIGURE 16. Multiple faults detection occurred at different time (a) the fault signals of sensor array, (b) the SPE statistic of fault detection, and (c) SPE contribution rates at different times.

TABLE 10. Error comparison of different fault recovery predictors.

ARE (%)	ELM	RVM
Impact	0.51	0.52
Broken-circuits	0.52	0.41
Overloading	0.51	0.40
Invalidating	0.52	0.42
Abnormal variance	0.51	0.43

Obviously, the training time of ELM is shorter than that of RVM. The reason has been discussed in section V.B.1.

However, when the sensor fault before concentration of the hydrogen changed, the RVM predictor in [11] will lose
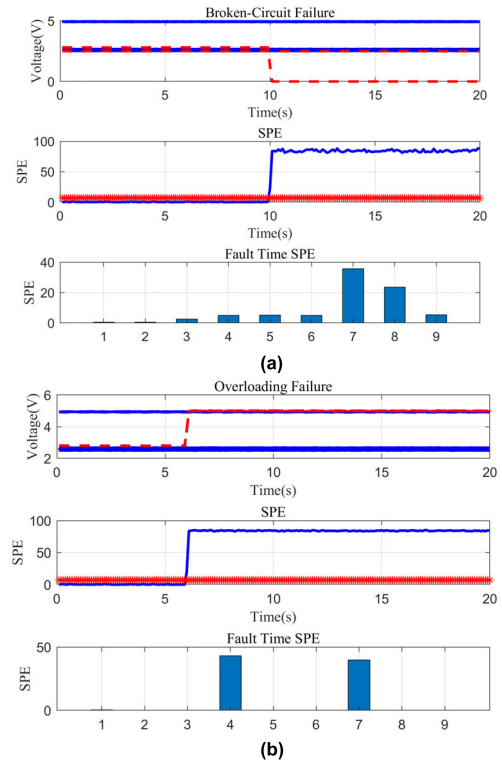

FIGURE 17. Multiple simultaneous faults detection (a) broken-circuit faults simultaneous occur in sensor S_7 and S_8 at 4 s and (b) overloading faults occur in S_4 and S_7 at 6 s.

its effectiveness, as well the ELM predictor can recovery the data at a high accuracy. Take MC109-1 as an example, the recovered curves are shown in Figure 19. The black curve is simulated as sensitive element MC109-1 overloading at 100 s while the concentration is changed at 150 s. The red curve which represented as the predicted result of ELM predictor is closed to the green curve, which represents the true data of MC109-1. The blue curve which means the result of RVM is closed to the initial data and do not changed with the changing of the concentration. The method in [11] is based on time series. The estimated value is based on historical data, which cannot give the subsequent information. In contrast, the relevance which includes the concentration information is used to build the recovery model in this paper. The changing of concentration can be calculated in real time.

2) IMPACT OF SENSOR NUMBER

The number of fault-free sensors that are employed to recover the faulty sensor output influences the recovery accuracy of the faulty data. Figure 20 shows the fault recovery results under different numbers of sensors.

Three different methods are considered. The application of 2 sensors in the experiment refers to using the same type sensors to the faulty sensor for the fault recovery. Utilizing 6 sensors means using the other different types of sensors for the fault recovery. Using 8 sensors means using all the fault-free sensors to recover the faulty one.
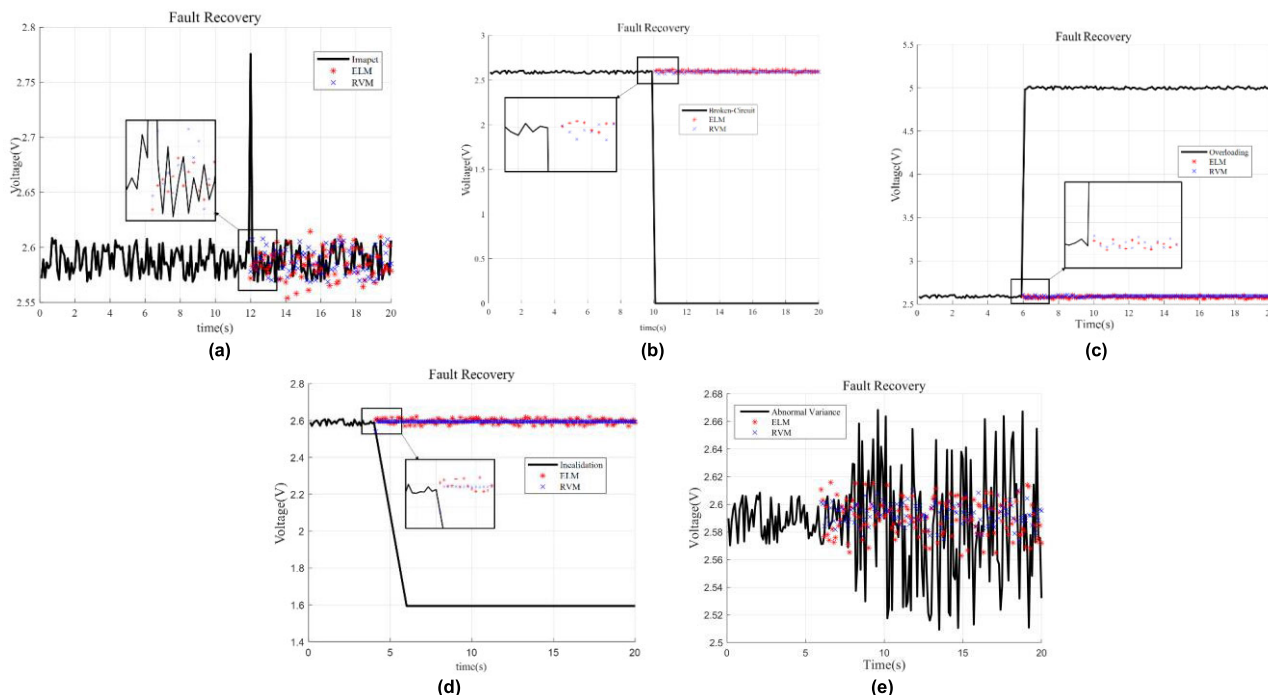
K. Song *et al.*: Fault Diagnosis and Reconfiguration Strategy for Self-Validating Hydrogen Sensor Array Based on MWPCA and ELM

IEEE *Access*

FIGURE 18. Sensor fault recovery using RVM and ELM (a) impact fault, (b) broken-circuit fault, (c) overloading fault, (d) invalidation fault, and (e) abnormal variance fault.
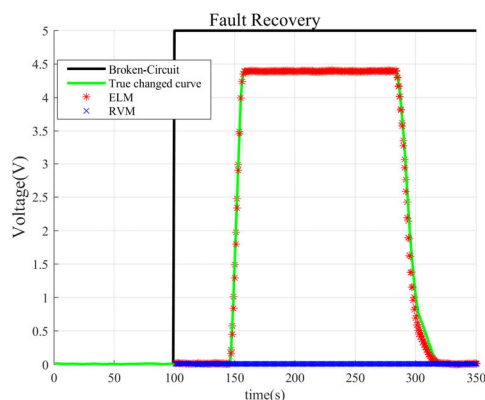

FIGURE 19. The comparison of ELM and RVM predictors for fault recovery when the concentration of hydrogen changed.

TABLE 11. Comparison results of sensor fault recovery by using different fault-free sensors.

No. of Sensors	2	6	8
Type	MC109-2, MC109-3	MQ8-1, MQ8-2, MQ8-3, MD61-1, MD61-2, MD61-3	The other 8 sensors
ARE（%）	0.82	11.82	0.55

In Figure 20 (a), over-loading fault happened in the catalytic combustion sensor MC109-1 (S_4). The method using 2 sensors is utilizing the same type sensor (MC109-2 (S_5) and MC109-3 (S_6)) to recovery the faulty sensor. The relevance of those two sensors is the largest to the faulty one. Therefore, the recover accuracy is higher. On the contrary, the method

using 6 sensors is utilizing different types sensors (MQ8-1 (MQ8-1 (S_1), MQ8-2 (S_2), MQ8-3 (S_3), MD61-1 (S_7), MD61-2 (S_8) and MD61-3 (S_9)) to the faulty one. The that of MC109-2 and MC109-3 to MC109-1. Compared with using 2 sensors, utilizing the other 6 sensors contains less relevant information. Therefore, the recover accuracy is lower. The method using 8 sensors contains all the relevance in the sensor array. Therefore, the accuracy is higher than the other 2 methods.

3) MULTI-FAULT RECOVERY
When multiple faults occur in the sensor array, fault recovery function is still effective by the correlation of fault sensors with the other fault-free sensors. Figure 21(a) shows the experimental results when broken-circuit faults simultaneous occur in sensor MD61-1 (S_7) and MD61-2 (S_8) at 10 s. The AREs of fault recovery using ELM are 0.95% and 0.92% overloading faults simultaneous occur in MC109-1 (S_4) and MD61-1 (S_7) at 6 s. recovery using ELM are 0.34% and 0.68% separately. Compared with single fault recovery, the precision of multiple fault recovery is almost same. Therefore, when multiple faults exist in the sensor array, the hydrogen concentration can still be measured by using the proposed fault recovery and regression strategy.

E. ABNORMAL FAULT DIAGNOSIS
1) FEATURE EXTRACTION USING MWPCA
The experiment of abnormal fault diagnosis of hydrogen sensor is conducted by using MWPCA feature extraction and ELM multi-classifier. Still taken the catalytic combustion hydrogen sensor MC109-1 (S_4) for example, the 5 faulty

IEEE *Access*

K. Song *et al.*: Fault Diagnosis and Reconfiguration Strategy for Self-Validating Hydrogen Sensor Array Based on MWPCA and ELM
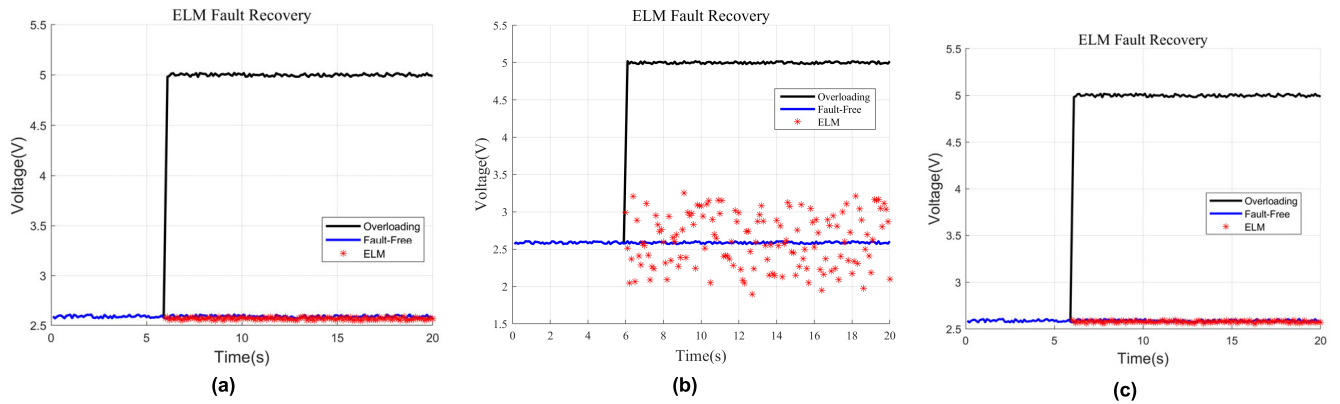

FIGURE 20. Sensor fault recovery using ELM under different numbers of fault-free sensors (a) over-loading fault recovery using 2 sensors, (b) broken-circuit fault recovery using 6 sensors, and (c) broken-circuit fault recovery using 8 sensors.
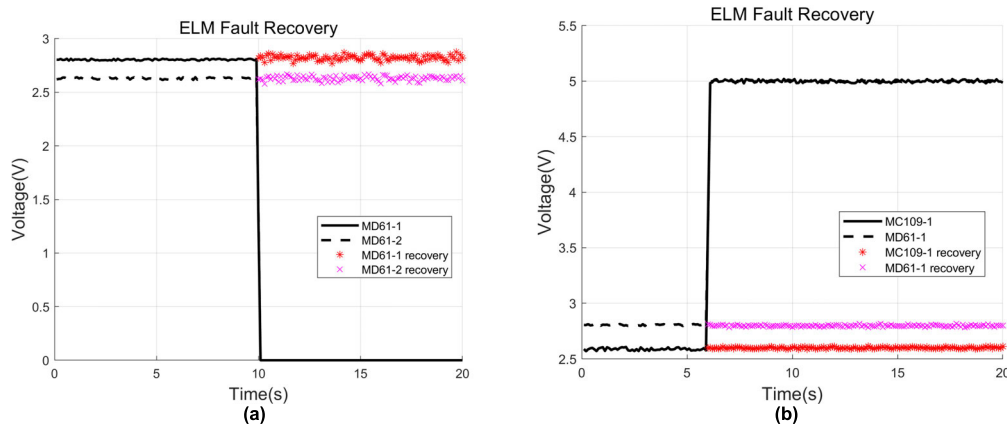

FIGURE 21. Multiple faults recovery using ELM.

TABLE 12. Comparison results of fault diagnosis using RBFNN, SVM and RVM multi-classifier.

Methods	Training sample	Testing sample	Training Time	Results of classification				
				Impact	Broken-circuit	Overloading	Invalidating	Abnormal variance
RBFNN	10×5	50×5	0.70 s	50	46	50	50	50
SVM	10×5	50×5	1.18 s	50	50	50	50	49
RVM	10×5	50×5	1.32 s	50	50	50	50	50
ELM	10×5	50×5	0.02 s	50	50	50	50	50

signals are measured at the hydrogen concentration of 5000 ppm and the extracted data length is 4 s. When the fault occurs, 4 second data around the fault occurrence time t_0 are acquired and sampling rate is 10 point/s. 20 samples of each fault are employed for feature extraction. As mentioned in Section IV.D, the extracted faulty features are injected into the RVM multi-classifier to execute fault diagnosis. Figure 22 shows the scatter plots of PC1 *vs* PC2 extracted by MWPCA. The contribution rate of PC1 is 72.9% and the contribution rate of PC2 is 18.8%, respectively.

2) ELM CLASSIFIER

The ELM multi-classifier is used to diagnose the sensor fault after feature extraction. Here, Sine kernel is selected as the

kernel function of ELM classifier and the kernel parameter is 10. Still taken the catalytic combustion hydrogen sensor MC109-1 (S_4) as an example, two groups of principle components (PCs) under each fault status are extracted in the experiment. 50 groups of fault samples are selected randomly to train the proposed ELM multi-classifier, and the remaining 250 groups are employed as the test samples.

Table 12 shows the fault diagnosis results under 5 different faults. It proves that ELM has a good prediction and generalization ability under small samples (The fault diagnosis rate is 100%). Obviously, RBFNN has the worst diagnosis rate due to the small training samples, while the proposed ELM multi-classifier has best accuracy and the training time. Particularly, this method is capable of achieving multi-fault
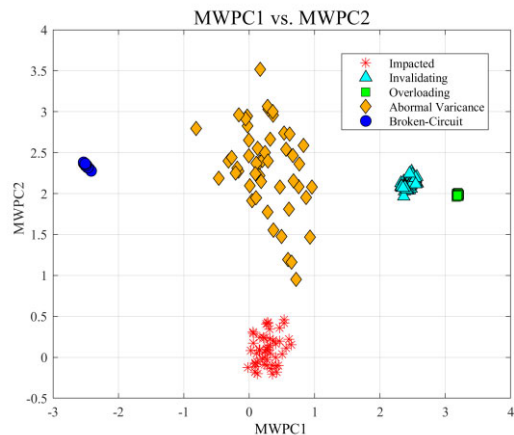
K. Song *et al.*: Fault Diagnosis and Reconfiguration Strategy for Self-Validating Hydrogen Sensor Array Based on MWPCA and ELM

IEEE *Access*

FIGURE 22. Scatter plots of PC1 vs PC2 extracted by MWPCA.

diagnosis when there are a variety of faults in the sensor array.

To sum up, the above experimental results indicate that this proposed methodology effectively achieves online concentration measurement, sensor fault detection, recovery and diagnosis, therefore improves the training time, accuracy and reliability of hydrogen sensor.

V. CONCLUSION
A novel fault diagnosis and reconfiguration strategy for self-validating hydrogen sensor is proposed in this paper. Hydrogen concentration estimation model under small sample calibration data is established based on ELM regression, which realizes rapid and precise quantitative measurement of hydrogen concentration, whose average relative error declined from 1.18% to 0.82% and the training time is shorten by an order of magnitude. Furthermore, online fault detection and fault recovery method on the basis of MWPCA and ELM is proposed, which solves the problem that the existing hydrogen detection system cannot simultaneously detect and recovery the multiple faults and improves the performance of fault isolation. Compared with the former time series method, the accuracy of fault recovery by utilizing this method is basically the same. this method solves the problem that the sensor cannot be effectively recovered when the concentration is changed. Additionally, fault diagnosis with the accuracy rate is 100% based on the proposed MWPCA feature extraction and ELM multi-classifier. Reducing or eliminating the influence of abnormal odor on fault detection will be researched in the future.

REFERENCES
[1] F. Falsafi, B. Hashemi, A. Mirzaei, E. Fazio, F. Neri, N. Donato, S. G. Leonardi, and G. Neri, "Sm-doped cobalt ferrite nanoparticles: A novel sensing material for conductometric hydrogen leak sensor," *Ceramics Int.*, vol. 43, pp. 1029–1037, Jan. 2017.

[2] K. Lakshmanan, A. M. Vijayakumari, and P. K. Basu, "Reliable and flow independent hydrogen sensor based on microwave-assisted ZnO nanospheres: Improved sensing performance under UV light at room temperature," *IEEE Sensor J.*, vol. 18, no. 5, pp. 1810–1819, Apr. 2018.

[3] G. B. Pour, L. F. Aval, and S. Eslami, "Sensitive capacitive-type hydrogen sensor based on Ni thin film in different hydrogen concentrations," *Current Nanosci.*, vol. 14, no. 2, pp. 136–142, Apr. 2018.

[4] G. B. Pour, "Electrical properties of the MOS capacitor hydrogen sensor based on the Ni/SiO$_2$/Si structure," *J. Nanoelectron. Optoelectronics*, vol. 12, no. 2, pp. 130–135, Feb. 2017.

[5] G. B. Pour and L. F. Aval, "Monitoring of hydrogen concentration using capacitive nanosensor in a 1% H-2-N-2 mixture," *Micro Nano Lett.*, vol. 13, no. 2, pp. 149–153, 2018.

[6] G. B. Pour and L. F. Aval, "Comparison of fast response and recovery pd nanoparticles and ni thin film hydrogen gas sensors based on metal-oxide-semiconductor structure," *Nano*, vol. 12, May 2017, Art. no. 17500968.

[7] T. Teutsch, N. Strohfeldt, F. Sterl, A. Warsewa, E. Herkert, D. Paone, H. Giessen, and C. Tarin, "Mathematical Modeling of a Plasmonic Palladium-Based Hydrogen Sensor," *IEEE Sensor J.*, vol. 18, no. 5, pp. 1946–1959, Mar. 2018.

[8] Z. Feng, Q. Wang, and K. Shida, "Design and implementation of a self-validating pressure sensor," *IEEE Sensors J.*, vol. 9, no. 3, pp. 207–218, Mar. 2009.

[9] M. P. Henry and D. W. Clarke, "The self-validating sensor: Rationale, definitions and examples," *Control Eng. Pract.*, vol. 1, no. 4, pp. 585–610, 1993.

[10] D. W. Clarke and P. M. A. Fraher, "Model-based validation of a DOx sensor," *Control Eng. Pract.*, vol. 4, pp. 1313–1320, Sep. 1996.

[11] Z. Shen and Q. Wang, "Failure detection, isolation, and recovery of multifunctional self-validating sensor," *IEEE Trans. Instrum. Meas.*, vol. 61, no. 12, pp. 3351–3362, Dec. 2012.

[12] Y. Chen, Y. Xu, J. Yang, Z. Shi, S. Jiang, and Q. Wang, "Fault detection, isolation, and diagnosis of status self-validating gas sensor arrays," *Rev. Sci. Instrum.*, vol. 87, pp. 211–221, Apr. 2016.

[13] J. Yang, Y. Chen, and L. Zhang, "An efficient approach for fault detection, isolation, and data recovery of self-validating multifunctional Sensors," *IEEE Trans. Instrum. Meas.*, vol. 66, no. 3, pp. 543–558, Mar. 2017.

[14] G. B. Huang, Q. Y. Zhu, and C. K. Siew, "Extreme learning machine: A new learning scheme of feedforward neural networks," in *Proc. IEEE Int. Joint Conf. Neural Netw.*, Jul. 2004, pp. 985–990.

[15] G.-B. Huang, Q.-Y. Zhu, and C.-K. Siew, "Extreme learning machine: Theory and applications," *Neurocomputing*, vol. 70, nos. 1–3, pp. 489–501, 2006.

[16] G. B. Huang, H. Zhou, X. Ding, and R. Zhang, "Extreme learning machine for regression and multiclass classification," *IEEE Trans. Syst. Man Cybern.-Syst.*, vol. 42, no. 2, pp. 513–529, Apr. 2012.

[17] B. Wang, L. Tang, J. Yang, B. Zhao, and S. Wang, "Visual tracking based on extreme learning machine and sparse representation," *Sensors*, vol. 15, pp. 26877–26905, Oct. 2015.

[18] J. K. Zhang, W. Yan, and D. M. Cui, "Concrete condition assessment using impact-echo method and extreme learning machines," *Sensors*, vol. 16, no. 4, pp. 447–464, 2016.

[19] Y. Jian, D. Huang, Y. Jia, K. Lu, Y. Huang, T. Wen, T. Zeng, S. Zhong, and Q. Xie, "A novel extreme learning machine classification model for e-nose application based on the multiple kernel approach," *Sensors*, vol. 17, no. 6, pp. 1434–1452, Jun. 2017.

[20] L. Zhang and D. Zhang, "Domain adaptation extreme learning machines for drift compensation in E-nose systems," *IEEE Trans. Instrum. Meas.*, vol. 64, no. 7, pp. 1790–1801, Jul. 2015.

[21] X. B. He and P. Y. Yu, "Variable MWPCA for adaptive process monitoring," *Ind. Eng. Chem. Res.*, vol. 47, pp. 419–427, Jan. 2008.

[22] M. Ammiche, A. Kouadri, and A. Bakdi, "A combined monitoring scheme with fuzzy logic filter for plant-wide tennessee eastman process fault detection," *Chem. Eng. Sci.*, vol. 187, no. 12, pp. 269–279, 2018.

[23] T. Zhang, C. Wang, J. Wang, Y. Chen, and Y. Zhang, "Moving window self-iteration PCE based OMA for slow linear time-varying structures," *J. Vibroeng.*, vol. 19, no. 6, pp. 4440–4458, May 2017.

[24] Q. Luo, Y. Peng, J. Li, and X. Peng, "MWPCA-ICURD: Density-based clustering method discovering specific shape original features," *Neural Comput. Appl.*, vol. 28, pp. 2545–2556, Sep. 2017.

[25] M. Jia, H. Xu, X. Liu, and N. Wang, "The optimization of the kind and parameters of kernel function in KPCA for process monitoring," *Comput. Chem. Eng.*, vol. 46, pp. 94–104, Jul. 2012.

[26] H. A. Nozari, M. A. Shoorehdeli, S. Simani, and H. D. Banadaki, "Model-based robust fault detection and isolation of an industrial gas turbine prototype using soft computing techniques," *Neurocomputing*, vol. 91, pp. 29–47, Sep. 2012.

[27] Y. Xiao, H. Wang, W. Xu, and J. Zhou, "L1 norm based KPCA for novelty detection," *Pattern Recognit.*, vol. 46, pp. 389–396, Jan. 2013.

IEEE *Access*

K. Song *et al.*: Fault Diagnosis and Reconfiguration Strategy for Self-Validating Hydrogen Sensor Array Based on MWPCA and ELM

[28] J. Pacheco, S. Casado, and S. Porras, "Exact methods for variable selection in principal component analysis: Guide functions and pre-selection," *Comput. Statist. Data Anal.*, vol. 57, pp. 95–111, Jan. 2013.

[29] K. Song, Q. Wang, Q. Liu, H. Zhang, and Y. Cheng, "A wireless electronic nose system using a Fe_2O_3 gas sensing array and least squares support vector regression," *Sensors*, vol. 11, no. 12, pp. 485–505, 2011.

[30] K. Song, B. Wang, M. Diao, H. Zhang, and Z. Zhang, "Fault detection and recovery for full range of hydrogen sensor based on relevance vector machine," *J. Harbin Inst. Technol.*, vol. 6, pp. 37–44, Jun. 2015.

[31] Z. Shen and Q. Wang, "A novel health evaluation strategy for multifunctional self-validating sensors," *Sensors*, vol. 13, pp. 587–610, Jun. 2013.

[32] Y. Chen, J. Yang, Y. Xu, S. Jiang, X. Liu, and Q. Wang, "Status self-validation of sensor arrays using gray forecasting model and bootstrap method," *IEEE Trans. Instrum. Meas.*, vol. 65, no. 7, pp. 1626–1640, Jul. 2016.

[33] K. Song, P. Xu, G. Wei, Y. Chen, and Q. Wang, "Health management decision of sensor system based on health reliability degree and grey group decision-making," *Sensors*, vol. 18, pp. 2316–2337, Mar. 2018.

[34] L. Zhang, F. Tian, C. Kadri, B. Xiao, H. Li, L. Pan, and H. Zhou, "On-line sensor calibration transfer among electronic nose instruments for monitoring volatile organic chemicals in indoor air quality," *Sens. Actuators B, Chem.*, vol. 160, no. 1, pp. 899–909, 2011.

[35] Q. P. Ha, H. Wahid, H. Duc, and M. Azzi, "Enhanced radial basis function neural networks for ozone level estimation," *Neurocomputing*, vol. 155, pp. 62–70, Sep. 2015.

YINSHENG CHEN received the M.S. and Ph.D. degrees in instrument science and technology from the Harbin Institute of Technology (HIT), Harbin, China, in 2011 and 2017, respectively. In 2017, he joined the School of Measurement and Communication Engineering, Harbin University of Science and Technology, as a Lecturer.

His current research interest includes intelligent sensor fusion technology.

TINGHAO ZHANG received the B.S. degree in instrument science and technology from the Harbin Institute of Technology (HIT), Harbin, China, in 2017, where he is currently pursuing the master's degree with the School of Electrical Engineering and Automation.

His current research interests include fault diagnosis and pattern recognition.

KAI SONG (M'12–SM'19) received the B.S., M.S., and Ph.D. degrees in instrument science and technology from the Harbin Institute of Technology (HIT), Harbin, China, in 2005, 2007, and 2011, respectively. In 2011, he joined the School of Electrical Engineering and Automation, HIT, as a Lecturer. He was a Visiting Scholar in electrical engineering with the University of Tokyo, Japan, from 2014 to 2015. He has been an Associate Professor with the School of Electrical Engineering and Automation, HIT, since 2016.

His current research interests include intelligent sensor systems and wireless power transfer.

GUO WEI received the B.S. and M.S. degrees in electromagnetic measurement and instruments from the Harbin Institute of Technology (HIT), China, in 1988 and 1991, respectively, and the Ph.D. degree in scientific research from Saga University, Saga, Japan, in 2003.

He is currently a Professor with the School of Electrical Engineering and Automation, HIT. His research interests include modern sensor technique, intelligent testing theory and its applications, weak signal detection and processing, wireless power transfer, and near field magnetic communication.

PENG XU received the B.S. degree in information engineering for smart grid from Zhejiang University (ZJU), Zhejiang, China, in 2011, and the M.S. degree in instrument science and technology from the Harbin Institute of Technology (HIT), Harbin, China, in 2014, where he is currently pursuing the Ph.D. degree with the School of Electrical Engineering and Automation.

His current research interests include prognostic and health management and intelligent sensing technology.

QI WANG (M'08) received the B.S. and M.S. degrees in electromagnetic measurement from the Harbin Institute of Technology, Harbin, China, in 1967 and 1980, respectively, where he is currently a Professor.

His research interests include intelligent testing instrumentation, information processing, sensor fault diagnosis, and the applications of artificial intelligence.

● ● ●